Proceedings of the Fortieth Turbomachinery Symposium
September 12-15, 2011, Houston, Texas

DEVELOPMENT OF A HIGH PRESSURE ROTORDYNAMIC TEST RIG FOR CENTRIFUGAL COMPRESSORS INTERNAL SEALS CHARACTERIZATION

Giuseppe Vannini
Senior Engineer
GE Oil&Gas Nuovo Pignone
Via Felice Matteucci, 2, 50127, Florence, Italy

Stefano Cioncolini
Engineering Manager
GE Oil&Gas, Nuovo Pignone
Via Felice Matteucci, 2, 50127, Florence, Italy

Vincenzo Calicchio
Lead Engineer
GE Oil&Gas, Nuovo Pignone
Via Felice Matteucci, 2, 50127, Florence, Italy

Francesco Tedone
Master Thesis Student
Dipartimento Ingegneria Meccanica, Nucleare e della Produzione, Pisa University
Largo Lucio Lazzarino,1 - Pisa - 56100 - Italy

Giuseppe Vannini is a Senior Engineer in the Advanced Technology Organization of GE Oil&Gas, which he joined in early 2001. He has been involved in advanced rotordynamics studies on high performance centrifugal compressors developing both analytical and experimental research activities. Recently he extended his activity to the design of prototypes for subsea compression applications (i.e. integrated high speed motocompressors). He holds a PhD in Mechanical Engineering at Pisa University and he's member of API684 Task Force.

Stefano Cioncolini is a Principal Engineer in the Technology Laboratory organization of GE Oil&Gas, which he joined in 1997. He has been involved in all the major validation programs of the last 14 years inside Organization, focusing his contribution in the Signal Processing, Special Instrumentation and Test Data Analysis. He holds a M.S. Degree in Physics at Florence University in 1992.

Vincenzo Calicchio is a Test Project Engineer in the Technology Laboratory organization of GE Oil&Gas. He joined GE in 2006. As technical coordinator, he has been involved in several validation programs, spreading from small components to full size turbines and compressors, from conceptual design to test execution and data analysis. Vincenzo holds a M. S. Degree in Mechanical Engineering at Naples "Federico II" University**.**

Francesco Tedone is currently completing his Master Degree course in Aerospace Engineering at Pisa University. The Master Degree Thesis work has been developed during his internship at General Electric Oil&Gas. This internship was possible thanks to the cooperation between GE Oil&Gas and Dipartimento di Ing. Meccanica Nucleare e della Produzione from Pisa University.

ABSTRACT

The current centrifugal compressor design for the Oil & Gas market is more and more challenging since the cost requirements and the presence of many competitors is pushing towards casing size reduction and rotational speed increase. The first requirement basically leads to increase the number of wheels per rotor and the second to cross more critical speeds requiring the proper degree of damping. The two consequences together lead also to increase the rotor flexibility ratio (defined as the ratio between the Maximum Continuous Speed and the first critical speed as per the Fulton diagram and API617 7th ed. [1-2]) and finally the rotordynamic stability is very much challenged.

The centrifugal compressors rotordynamic stability is then strictly related to the internal seals' dynamic behaviour and for this reason the authors' Company decided several years ago to develop internally a High Pressure Seal Test Rig to measure seals' stiffness and damping. The rig is now in operation. This paper aims to describe the main test rig capabilities, the applied identification procedures and the preliminary test results on a long labyrinth seal (smooth rotor - straight toothed stator).

Due to the pressure level (500bar design pressure), the test rig plant appears like a high-pressure industrial plant equipped with the testing cell (a 1:1 scale high pressure compressor) and all the relevant auxiliaries: a 400 kW electric motor (driven by a VFD), a speed increaser gear box, a high pressure reservoir (6

Copyright © 2011 by Turbomachinery Laboratory, Texas A&M University

m^3) with a volumetric compressor to fill it, high pressure pipes and valves.

The testing cell is composed of a high-pressure compressor casing with stator parts capable to regulate the seal inlet swirl and a rotor running on Active Magnetic Bearings (AMBs), which serve as exciters (5kN MAX Force over a 0-330 Hz frequency range per axis) and displacement transducers. Special instrumentation is installed into the testing cell in order to measure the main test parameters: seal upstream/downstream gas pressure, upstream temperature and swirl and mass flow.

Industrial high-pressure instrumentation is installed on the plant for regulation and monitoring purpose.

Maximum test pressure is 350bar and maximum rotational speed is 15000rpm. Test gas is nitrogen.

The AMBs control-system capabilities have been tuned to define several alternative excitation patterns and the relevant state of the art identification techniques have been applied.

The first seal tested is a long labyrinth seal to simulate a centrifugal compressor balance piston seal. Test results and comparison with a commercial bulk flow code predictions will be fully described.

Finally, the future test program will be showed.

INTRODUCTION

Annular seals used in turbomachinery and especially in process centrifugal compressor are key elements for smooth machine operability since their effect on the rotordynamics is absolutely not negligible. Annular seals' behaviour is strictly related to the compressor load and their proper design can really make the difference in terms of rotordynamic stability. There are many well known reference cases which clearly demonstrate that the instability due to seals destabilizing forces is real: the Kaybob (Smith, 1975) and the Ekofisk (Cochrane, 1976) compressors were the forerunners in this kind of documented field issues but many others papers followed (there are examples coming from almost all the OEM companies and several End Users).

As a consequence both the academic and industrial research started and after some years led to very important milestones in the turbomachinery engineering field.

Major Universities developed numerical tools to compute the stiffness and damping of these elements in order to simulate their effects on the rotordynamic stability: Iwatsubo (1984) was among the first people to publish about the bulk flow model approach which is till now the more time effective numerical approach for computing stiffness and damping. After that Childs and Scharrer (1986) started a long record of papers published by Turbomachinery Laboratory in the seal modelling field: in addition to the numerical aspects these works have the big plus of the in-house experimental validation.

In fact at the same time experimental facilities were built and after some years they become the source of validation for these numerical tools.

In the labyrinth seals field Childs and Scharrer (1986), as already said, started to show the first experimental results and later on Picardo and Childs (2005) compared the labyrinth seal rotordynamic experimental behaviour with both the relevant predictions and with a damper seal dynamic behaviour.

Also the industry moved directly in the seals' rotordynamic research field tackling the problem either at component or at system level.

At component level the focus was on the single seal dynamic characteristics and for this reason dedicated test rigs were built. The most relevant example according to the authors' knowledge is the Wagner (1996) reference where it is showed a very sophisticated test rig equipped for the first time with in-house developed AMBs and rated for 250bar pressure. In Wagner N., R. Gaussmann, (2009), the same upgraded rig was able to test impeller eye labyrinth seal thanks to the very accurate measurement methodology which was put in place by the authors.

At system level the focus was on the measurement of the system logarithmic decrement and on the understanding of the impact of the annular seals on such stability indicator. Baumann (1999) was probably the first to accomplish such a task by using a magnetic exciter installed on one compressor shaft end, which was shaking asynchronously the rotor and inducing the relevant response. For the first time it was proven that the seals are effective not only on system damping but even on system stiffness reducing the first rotor natural frequency. Moore (2002) showed a similar stability testing performed on a centrifugal compressor equipped with a damper seal; this time the stability was improving at higher load due to the beneficial effect of this special kind of seal.

Despite this combined analytical-experimental effort, the current predictability of the tools cannot be considered very high or, at least, no common basis exists for a stability assessment. On this regard Kocur and Nicholas (2007) showed the results of a survey conducted among the main OEMs, Academies and Consulting companies where the different rotordynamic coefficients predictions of the same journal bearings and labyrinth seals led to a big scatter in terms of rotor final log dec (-1 ÷ +1 log dec range).

In addition to this, also the major Oil&Gas Industry standard (API617, Standard for Process Centrifugal Compressors Design) finally allows each manufacturer to prove the soundness of the rotordynamic design based on his own experience more than on some standard criteria.

Due to all these reasons since many years the authors' company decided to develop a deep internal knowledge in seal rotordynamics. A specific project aimed to setup a dedicated and permanent rotordynamic seal test rig was launched. This rig is now operational, and the present paper will give a full description of its current capabilities, show the present results (relevant to a long labyrinth seal) and illustrate the future test plan.

Copyright © 2011 by Turbomachinery Laboratory, Texas A&M University

TEST RIG DESCRIPTION

The seal test rig is actually a small plant and the relevant description will be divided in two main areas:

- Test Cell
- Test Loop

Test Cell

The Test Cell is the heart of the plant since it contains the seals, which are the object of this test, and the instrumentation directly involved in the seal coefficients measurement.

From an external look it seems like a real barrel centrifugal compressor (see Figure 1) since the external casing is the same as a high-pressure compressor (400bar is the design pressure).

Figure 1 – Test Cell.

The external casing envelops the bundle, made of four big flanges and containing the test seals, the AMBs and the instrumentation and finally the rotor with the relevant torque transmission system. Figure 2 shows the main items of the Test Cell mentioned above.

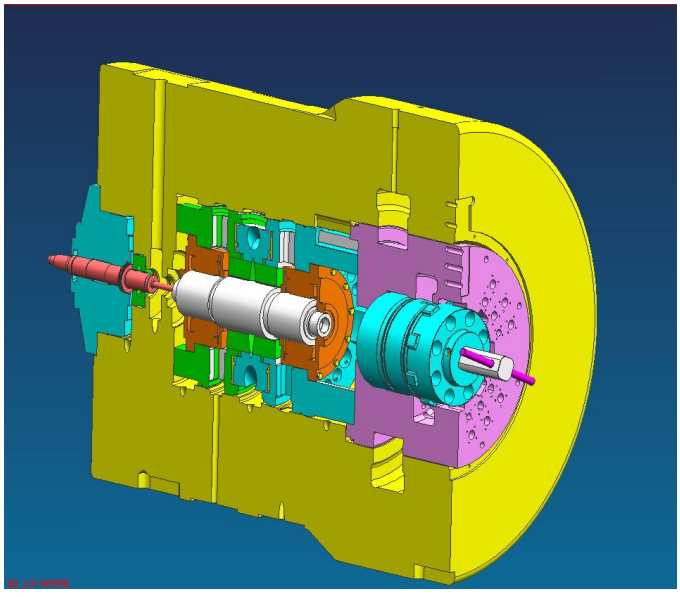

Figure 2 – Test Cell internals 3D view.

Of special interest is the internal bundle (see Figure 3) which is pre-assembled with all the relevant instrumentation and which is finally inserted into the casing through a special tool: a sliding carriage which allows to support the heavy weight of the bundle (1.85t) and to guarantee the required fitting precision (assembly clearances in the order of few tenths of millimeter).

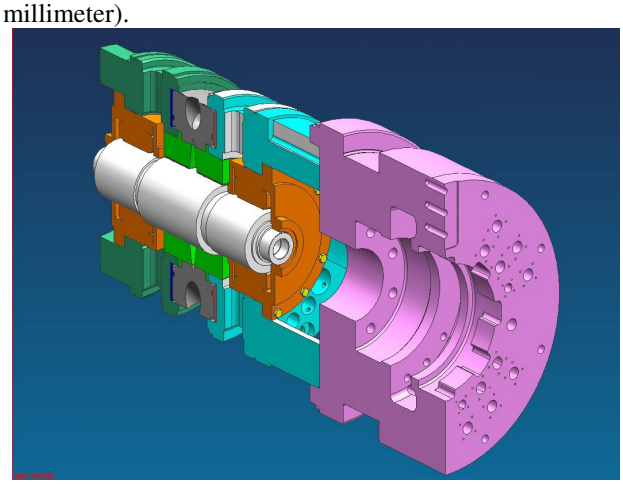

Figure 3 – Internal Bundle 3D view.

The internal bundle is assembled stacking together up to 4 parts (refer to Figure 3):

- The head cover (pink part)
- The external flange (turquoise part) with the AMB#24 (not drive end bearing, orange part)
- The swirler ring (gray part) which is capable to impose to the gas an inlet tangential velocity upstream the seal
- The internal flange (dark green part) with the AMB#13 (drive end bearing, orange part)

The swirler ring is provided with four axisymmetric nozzles, which boost the gas from the inlet plenum to the seal upstream volume. This annular shaped cavity helps to uniform the gas velocity before the seal entrance. The aspect ratio (radial length / axial width) of this cavity is about 4 and it is made with a trapezoidal section to allow a constant radial gas velocity. The swirler ring provides a gas velocity at seal inlet, which is almost constant and independent from the rotational speed and inlet pressure level. The current preswirl ring was designed for a medium-high preswirl: 0.85 @ 10krpm. The preswirl value is measured through static and total pressure measurements at seal inlet and mass flow measurement. The total pressure probes are installed as near as possible to the seal inlet (they are located approximately in the mid of seal ring radial thickness).

The test seals (green parts) are mounted on the two flanges in a back-to-back arrangement.

The rotor is made of:

- Main rotor (white part of Figure 3), which is a rigid hollow shaft having a central part with a calibrated diameter for the test seal, the AMBs laminations and the auxiliary bearing sleeves.
- Quill shaft (red part in Figure 2) which is flexible enough in bending direction to disconnect the lateral vibration of the main rotor from the driver but robust enough in torsional direction to transmit the driving torque.
- Interconnecting shaft (red part in Figure 2), which is bolted to the quill shaft at one side and coupled through a flexible coupling to the gearbox at the other side. This shaft is running on high-speed ball bearings, which serve also as

Copyright © 2011 by Turbomachinery Laboratory, Texas A&M University

thrust bearings for the rig being of angular contact type. In fact, even if the thrust is minimized by the seals back-to-back arrangement, a residual thrust still exists due to a potential pressure unbalance between the volumes downstream the seals and to the presence of the quill shaft diameter.

Finally the region downstream the seal is a wide-open cavity connected to the atmosphere through a control valve that is regulating the pressure ratio. At the same time the volume downstream the AMBs is connected to the atmosphere in order to have a cooling flow in all the test conditions.

The seal test rig operating characteristics are:

- Maximum inlet pressure: 350bar
- Outlet pressure: tunable to reach maximum 2.5 as a pressure ratio.
- Rotational speed: up to 15krpm
- Excitation through AMBs: frequency up to 250Hz, dynamic load up to 5kN and capability to impose linear or orbital excitations
- Test gas is nitrogen

Instrumentation

The testing cell is equipped, in every section, with proper instrumentation, aimed to monitor all the relevant test parameters (static and total pressures and temperature).

Due to the high-pressure level and to assembly constrains, not only commercial instrumentation has been used but also customized probes (total pressure and temperature) have been installed.

Test Loop

The whole test bench can be seen as a real high-pressure plant (piping rating: API 10000).

All the equipments and their installation are PED compliant.

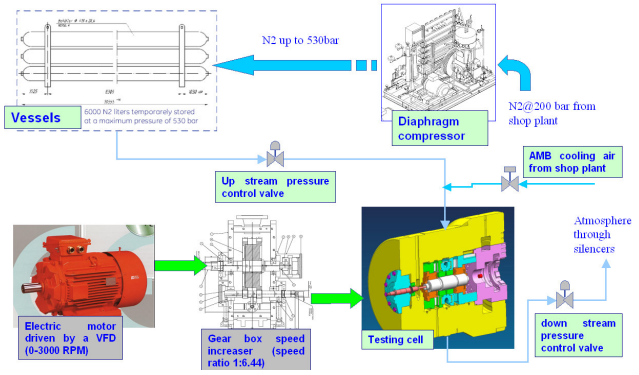

Figure 4 – Test Rig layout.

The main purpose of the test loop is to feed the test cell with nitrogen at the proper pressure level.

The main items of the loop (see Figure 4) are:

- Diaphragm Compressor: which is needed to raise the pressure level above 200bar (maximum pressure from the internal grid) and to feed the reservoir.
- High-pressure reservoir: it is a 6m^3 modular reservoir, which stores the nitrogen needed for the test.
- Electric motor and gearbox.

High-pressure industrial transducers (periodically calibrated) have been installed for plant monitoring and operability.

The basic concept of the test bench is to fill the pressure reservoir with nitrogen at high pressure and then discharge the nitrogen into the testing cell.

The pressure reservoir is directly fed by the nitrogen shop plant up to 200bar; then in order to increase the pressure from 200bar up to 500 bar the nitrogen supply is routed to the suction of the diaphragm compressor which allows reaching the higher pressure levels.

During the test, the pressure at the testing cell inlet and outlet section is kept at the desired levels by two pressure control valves. The valves are managed, from the test bench UCP, with two separates PID controllers.

The whole plant, for safety reasons, is located in a safe area, delimited with a concrete wall (3m height, 0.3m thickness). Before starting the test sequences, and after the last inspection of the area, the main gate is closed and the proper LOTO standards are applied.

The complete test sequence, therefore, is remote-managed, from the nearby control room, by means of the UCP and the proper control software.

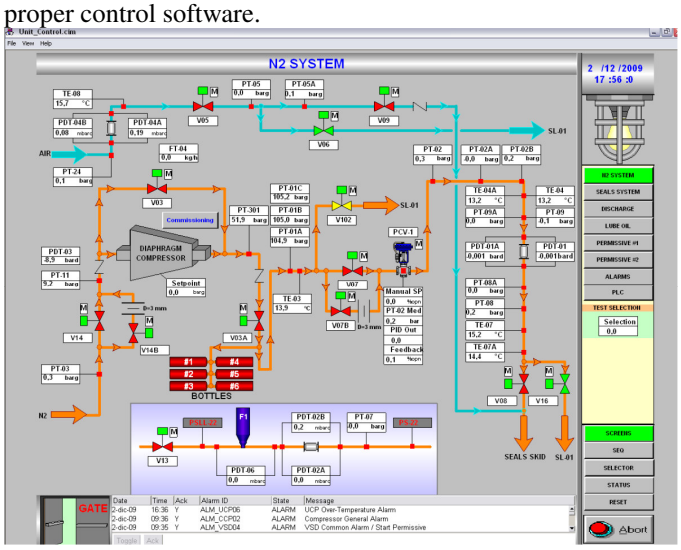

Figure 5 – Control System HMI.

The control software has been built in order to meet the test sequences and, above all, the safety requirements both for people and equipment. It has been debugged and tuned using a mono-dimensional dynamic model of the complete test loop, developed on purpose.

Particular attention has been paid for safety and emergency sequences.

Control software and bench operability have been fine tuned during the final commissioning.

TEST PROCEDURE

The complete test sequence can be described with the following steps:

- Vessel pressurization up to 200 bar from the shop plant
- Vessel pressurization up to pressure set point (between 200 and 500bar) by means of the diaphragm compressor
- AMBs cooling air activation
- AMBs start and levitation
- *0 rpm orbit tuning*

Copyright © 2011 by Turbomachinery Laboratory, Texas A&M University

- Gear Box lube oil start
- Ball bearings oil mist lubricator start
- Motor start up to reach speed set point
- *Nominal speed base line 1*
- Whole testing cell pressurization up to backpressure set point
- *Pressure baseline 1*
- Upstream pressurization up to test set point and backpressure kept at test set point (both PCVs in control)
- *Experiment (data for seal coefficients extraction)*
- Whole testing cell depressurization up to backpressure level
- *Pressure baseline 2*
- Testing cell total depressurization and cooling air activation
- *Nominal speed baseline 2*
- Electric motor stop
- AMBs control system stop

A typical test procedure diagram is showed in Figure 6.

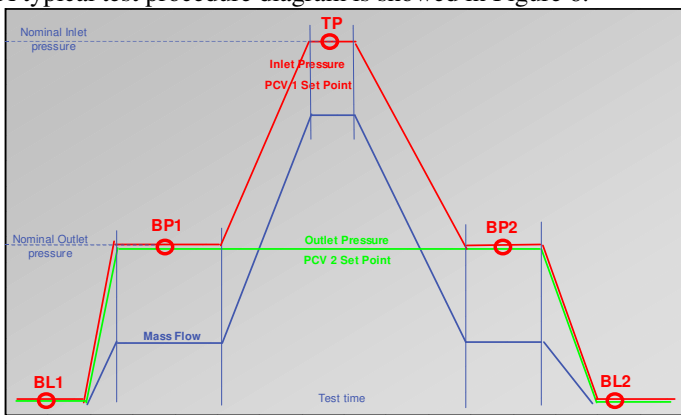

Figure 6 – Test Procedure diagram.

Depending on the test point pressure levels, the steady testing time varies; the higher the pressure level, the shorter the testing time. The typical testing time at high pressure (more than 200bar) is 30sec.

TEST HARDWARE

The seal under test is a long labyrinth seal that is representative of a balance piston seal for a medium pressure, medium size barrel centrifugal compressor. The labyrinth seal is shown in Figure 7 and it is characterized by the following features:

- 14 statoric teeth
- No shunts nor swirl brakes
- Nominal rotor diameter: 220mm
- Nominal radial clearance: 0.3mm

The decision to start the testing activity with this specific seal is mainly because of the following reasons:

- The frequency dependence is theoretically limited.
- The sensitivity to taper and static offset is theoretically negligible.

These two reasons in fact relaxed the requirements for both the experiment and the relevant postprocessing allowing to have a "soft start". On the opposite side, the experiment was more challenging in terms of sensitivity since the labyrinth seal coefficients are the lowest among all the typical seals of interest (honeycomb or pocket damper seals).

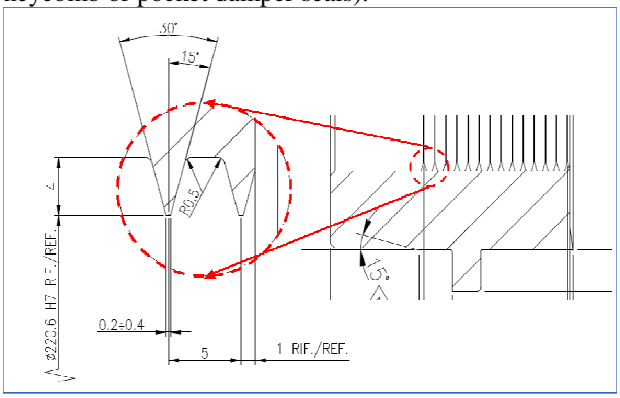

Figure 7 – Labyrinth seal drawing details.

IDENTIFICATION METHODOLOGY

Identification methodology is a very critical aspect of the data postprocessing since it defines the transfer function, which yields the final seal dynamic coefficients. The current mathematics was developed starting from the open literature (main sources were Wagner, 1996 and Rouvas-Childs, 1993) and then tailored for the specific needs of the test rig.

More specifically as a first step the equations of motion (Eq. 1) for the main rotor are defined (assuming a cylindrical motion so only 2 translatory degrees of freedom are considered).

$$\begin{cases} F_{bx} + F_{kx} + F_{cx} = M_R \ddot{x}/2 \\ F_{by} + F_{ky} + F_{cy} = M_R \ddot{y}/2 \end{cases} \quad (1)$$

An important point in Eq. (1) is that it is referred to a single AMB assuming that either the bearing forces or the seal forces are the same between the two AMBs. This is almost always true due to the excitation methodology, which aims to have a cylindrical motion in the test rotor. The equations are solved for each of the two bearings separately (AMB#13 and AMB#24) and then averaged for the final results.

Excitation forces are applied through the AMBs and they are harmonic with a content of 5 different tones, Eq. (2a) and the relevant displacement Eq. (2b) are harmonic as well with the same frequency content:

$$\begin{cases} F_{bx} = F_{bx0} e^{j(\Omega t + \Phi_{bx})} \\ F_{by} = F_{by0} e^{j(\Omega t + \Phi_{by})} \end{cases} \quad (2a)$$

$$\begin{cases} x = x_0 e^{j(\Omega t + \Phi_x)} \\ y = y_0 e^{j(\Omega t + \Phi_y)} \end{cases} \quad (2b)$$

Seals are modeled with the classical stiffness and damping matrices. Moreover these matrices are considered skew symmetrical as a first approach (Eq. 3). This is another important assumption, which was made in order to start the mathematics development (a reasonable assumption for the labyrinth seal under testing). Anyway the mathematics is going to be improved to take into account eight independent stiffness and damping coefficients.

Copyright © 2011 by Turbomachinery Laboratory, Texas A&M University

$$-\begin{bmatrix} F_{KX} \\ F_{KY} \end{bmatrix} = \begin{bmatrix} K_{XX} & K_{XY} \\ K_{YX} & K_{YY} \end{bmatrix} \cdot \begin{bmatrix} x \\ y \end{bmatrix} = \begin{bmatrix} K & k \\ -k & K \end{bmatrix} \cdot \begin{bmatrix} x \\ y \end{bmatrix}$$
$$-\begin{bmatrix} F_{CX} \\ F_{CY} \end{bmatrix} = \begin{bmatrix} C_{XX} & C_{XY} \\ C_{YX} & C_{YY} \end{bmatrix} \cdot \begin{bmatrix} \dot{x} \\ \dot{y} \end{bmatrix} = \begin{bmatrix} C & c \\ -c & C \end{bmatrix} \cdot \begin{bmatrix} \dot{x} \\ \dot{y} \end{bmatrix} \quad (3)$$

If Eq. (2a), (2b) and (3) are substituted into Eq.(1) and everything is divided by the relevant displacement terms the following Transfer Functions equations are derived:

$$2\left[\frac{F_{bx0}}{x_0}\frac{e^{j\Phi_{bx}}}{e^{j\Phi_x}} - K - k\frac{y_0}{x_0}e^{j(\Phi_y-\Phi_x)} - j\Omega C - j\Omega c\frac{y_0}{x_0}e^{j(\Phi_y-\Phi_x)}\right] = -M_R\Omega^2$$

$$2\left[\frac{F_{by0}}{y_0}\frac{e^{j\Phi_{by}}}{e^{j\Phi_y}} - K + k\frac{x_0}{y_0}e^{j(\Phi_x-\Phi_y)} - j\Omega C + j\Omega c\frac{x_0}{y_0}e^{j(\Phi_x-\Phi_y)}\right] = -M_R\Omega^2 \quad (4)$$

Separating into Real and Imaginary parts we have 4 equations:

$$\left[\frac{F_{bx0}}{x_0}\cos(\Phi_{bx}-\Phi_x) - K - k\frac{y_0}{x_0}\cos(\Phi_y-\Phi_x) + \Omega c\frac{y_0}{x_0}\sin(\Phi_y-\Phi_x)\right] = -\frac{M_R\Omega^2}{2} + \frac{F_\varepsilon}{x}$$

$$\left[\frac{F_{bx0}}{x_0}\sin(\Phi_{bx}-\Phi_x) - k\frac{y_0}{x_0}\sin(\Phi_y-\Phi_x) - \Omega C - \Omega c\frac{y_0}{x_0}\cos(\Phi_y-\Phi_x)\right] = \frac{F_\varepsilon}{x} \quad (5a)$$

$$\left[\frac{F_{by0}}{y_0}\cos(\Phi_{by}-\Phi_y) - K + k\frac{x_0}{y_0}\cos(\Phi_x-\Phi_y) - \Omega c\frac{x_0}{y_0}\sin(\Phi_x-\Phi_y)\right] = -\frac{M_R\Omega^2}{2} + \frac{F_\varepsilon}{y}$$

$$\left[\frac{F_{by0}}{y_0}\sin(\Phi_{by}-\Phi_y) + k\frac{x_0}{y_0}\sin(\Phi_x-\Phi_y) - \Omega C + \Omega c\frac{x_0}{y_0}\cos(\Phi_x-\Phi_y)\right] = \frac{F_\varepsilon}{y} \quad (5b)$$

Equations (5a) are relevant to the horizontal equilibrium (Real and Imaginary part) while equations (5b) are relevant to the vertical equilibrium (Real and Imaginary part). This system of equations has 4 basic unknowns (the seal coefficients) while all the remaining values are measured quantities: the terms F_ε/x, F_ε/y are considered as a mismatch between the excitation forces and the inertia forces and can be evaluated during the baseline. The system can be finally solved for the 4 unknown coefficients.

$$[A]_{(\exp)} \cdot \begin{bmatrix} K \\ k \\ C \\ c \end{bmatrix} = [B]_{(\exp)} + [F_\varepsilon] \quad (6)$$

Before getting the seal coefficients, the identification procedure invokes the baseline computation. The baseline is fundamental to check the status of force and displacement sensors and to correct for some not identified phenomena that can occur during the preliminary rotation with low-pressure gas. Finally, the known terms vector is fully identified thanks to the baseline (assuming the coefficients are nil):

$$[B]_{(baseline)} + [F_\varepsilon] = 0 \quad (7a)$$

$$[B]_{(seals)} = [B]_{(\exp)} - [B]_{(baseline)} \quad (7b)$$

The final coefficients are extracted by inversion of the following matrix:

$$\Rightarrow \begin{bmatrix} K \\ k \\ C \\ c \end{bmatrix}_{(seals)} = \left([A]_{(\exp)}\right)^{-1} \cdot [B]_{(seals)} \quad (8)$$

In order to get different sets of test data for the same seal different excitation patterns have been implemented in the test execution protocol:

- Vertical linear orbit
- Horizontal linear orbit (4)
- Forward + Backward circular orbits

As said at the beginning of the paragraph this postprocess methodology was developed at first but a more advanced one is going to be developed to take into account all the eight independent seal coefficients and to avoid the averaging between the two AMBs contributions. The test results showed in the results paragraph will be based on the methodology stated in this paragraph.

DATA ACQUISITION AND DATA POSTPROCESSING

Data Acquisition System

The acquisition system used to perform the experiment was divided mainly in the following portions.

1. The low-speed (static) portion was designed to collect all the process parameters; specifically gas temperatures, pressures, mass flow and other auxiliaries' functional parameters.
2. The high-speed (dynamic) portion was designed to measure the displacements of the rotor and the forces actuated by the Active Magnetic Bearings on the rotor.
3. The signal generation portion is able to generate 4 independent waveforms driving the Active Magnetic Bearings to force the rotor on the desired whirl orbits.

The low-speed system is based on a commercial PLC able to sample data at 10 Sa/s with the main function to monitor the parameters, set the correct upstream and downstream pressures and control the rotor speed.

The dynamic portion, together with the generation portion is the core of the Data Acquisition System. It is based on the National Instrument HW PXI 4472, able to perform an acquisition with 24 bit of resolution with simultaneous sampling at 102.4 KSa/s. Due to the bandwidth of interest, the sampling rate was set at 5 KSa/s.

The generation of 4 independent waveforms is based on the National Instrument HW PXI 6713, able to generate eight independent waveform with 1 MSa/s.

The system is then based on a proprietary software; the main feature of the software is to generate a square reference signal and relate to this signal for each axis several sinusoidal waveform with frequency multiple of the reference. Then the waveforms can be shifted with a phase control one respect to the other in order to achieve vertical whirl, horizontal whirl, circular forward or circular backward whirl. The flow diagram describing the data acquisition system is shown in Figure 8).

Copyright © 2011 by Turbomachinery Laboratory, Texas A&M University

Signal postprocessing

One of the most important parts developed to allow the seal coefficient determination is the signal post processing.

The post processing is divided into 2 main parts: the first is performed on line and is related to all the signal computation in term of Fourier filtering, Fourier transformation, orbit creation and transfer function computations (e.g. the Active Magnetic Bearing force computation); the second is related to the solution of the mathematic equations, the dynamic correction due to the stator vibration and the uncertainty computation.

Online postprocessing

The basic principle is to have in real time some computed parameters useful to control the quality of the experiment like:

- Rotor Orbits: to check their shape and to compare them between the two bearings (to avoid a rotor conical motion)
- The inertia force balance before the gas injection to check the system baseline behaviour

The first online computed parameter is the applied force. This computation is performed both in real time and in postprocessing to have the force signal ready for setting and monitoring during the experiment.

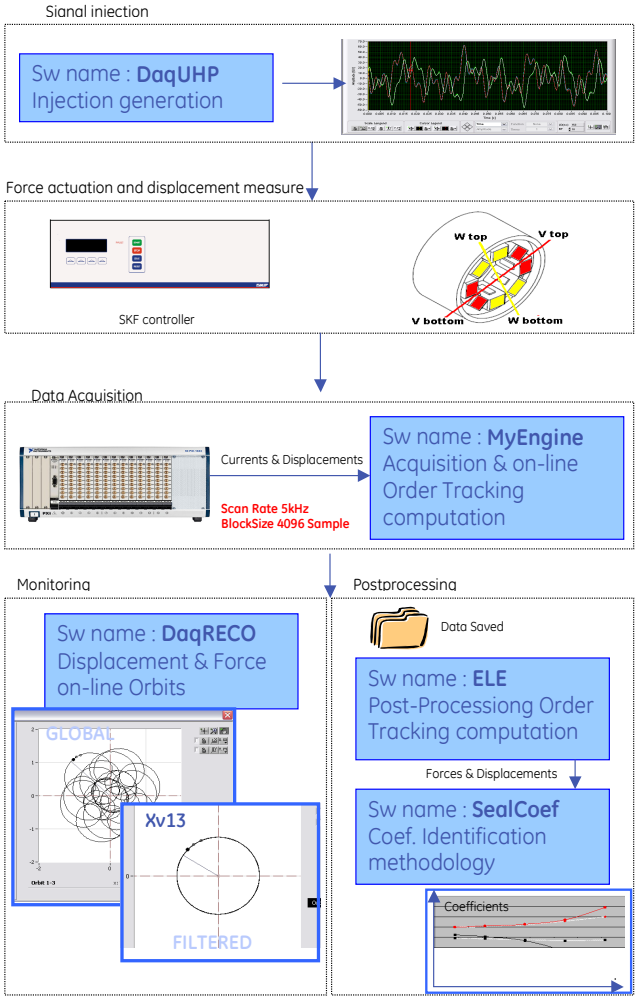

Figure 8 – Data Acquisition System Flow diagram.

The computation is based on the classical formulation used in literature that does not take in account the iron saturation:

$$F = \mu_0 N^2 A_t \left\{ \left[\frac{I_{top}}{2(g-x)} \right]^2 - \left[\frac{I_{bottom}}{2(g+x)} \right]^2 \right\} \quad (9)$$

A very accurate definition of the Active Magnetic Bearing geometry and properties of the Iron of both the core and the shaft allows improvements on this formulation. In details the Active Magnetic Bearings used have the following characteristics.

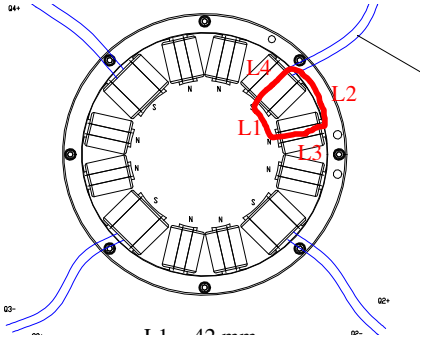

Figure 9 – AMB scheme for inductance calculation.

	Imperial Units		Metric Units	
1.0 Bearing Geometry				
See Drawing No.	856-0052-001 (GENP-003-M-A) Stator Stack SA			
Number of Poles per Quadrant	3			
Stator OD	11.417	in	290.00	mm
Stator ID	5.984	in	152.00	mm
Back Iron Width	0.787	in	20.00	mm
Pole Height	1.968	in	50.00	mm
Pole Width	0.726	in	18.44	mm
Pole Offset Angle	25.28	deg	0.44	rad
Slot Width (@ ID)	0.591	in	15.00	mm
Stator Stack Length	3.937	in	100.00	mm
Rotor OD	5.906	in	150.00	mm
Rotor Lamination ID	1.262	in	32.05	mm
Nominal Gap	40	mils	1.00	mm
2.0 Material Selection				
Stator Material Grade	M-19, C-5, 0.014 in			
Rotor Material Grade	ARNON 5, C-5, 0.005 in			
3.0 Coil Specification				
See Drawing No.	856-0052-001 (GENP-003-M-A) Stator Stack SA			
Wire Type	Phelps Dodge TZQS or Equivalent/Better			
Wire Gage	8	AWG		
Number of Turns per Pole	26			
Quadrant Resistance	0.043	Ohms		
Min. Pole Clearance (@ centre of pole)	0.050	in	1.27	mm
Max. Coil Extension on lead exit side	0.500	in	12.70	mm
Max. Coil Extension non lead exit side (Including Insulation)	0.500	in	12.70	mm
Coil Layout	2 layers x 13 turns			
4.0 Coil Insulation and Potting				
Insulation Temperature Class	Class F / 311°F		Class F / 155°C	

Table 1 – AMB general characteristics.

Using these parameters we substituted the g constant with the following effective gap to take care of the iron saturation.

Copyright © 2011 by Turbomachinery Laboratory, Texas A&M University

$$g_{effective} = g + \frac{L1}{2\mu_r^{ARNON}} + \frac{L2+L3+L4}{2\mu_r^{M19}}$$

$$H = \frac{NI}{L} = \frac{NI}{L1+L2+L3+L4}$$

$$\mu_r = \frac{B}{H * \mu_0} = see\_table \tag{10}$$

For the core M19 material we extracted from the B-H curves the following dependence:

$$\mu_r^{M19} = \frac{0.55*10^6}{H^{0.89}} \tag{11}$$

For the rotor material Arnon5 from the B-H curves the following dependence

$$\mu_r^{ARNON5} = \frac{0.55*10^6}{H^{0.89}} \tag{12}$$

Using these relations the effective gap is a function of the currents linked to each expansion. The formulations, as demonstrated in the calibration section are able to take care of the saturation.

At this step, the major parameters to compute the sealing coefficients are ready for further computations; in more details they are the time waveform of the rotor displacements respect to the casing and the forces applied by the Active Magnetic Bearings on the rotor. In addition, other dynamic pressure transducers installed inside the barrel are recorded, but they will not be discussed in detail inside this paper.

The second real time computation performed starting from the time domain waveforms is the **amplitude spectrum computation**; this representation allows investigating the signal components in the frequency domain very easily, and even in real time.

To have the proper resolution with a good response to the transient the block size of the data used to perform the FFT computation was 4096; with a Sampling Rate of 5Ksa/s the window of data used to generate the amplitude spectrum is 0.8s long with a resolution of 1.25 Hz.

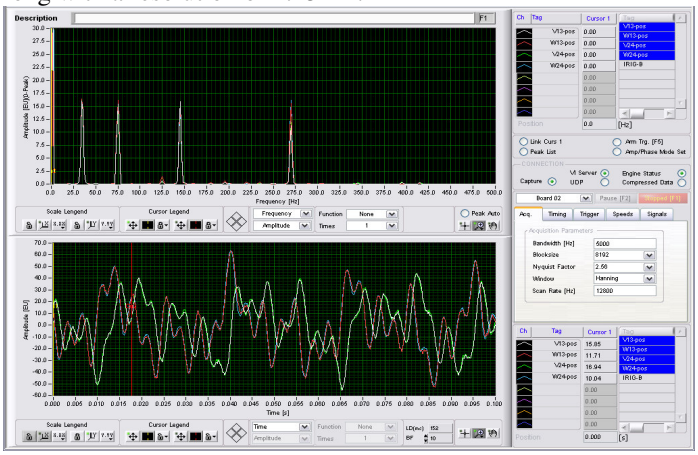

Figure 10 – Amplitude spectrum from time signal.

This setting allows to discriminate the injected frequencies and follows the rapid changes during the setting of the experiment.

The third real time computation performed, starting again from the time domain waveforms, is the **digital vector filtering**. This computation is based on the **Fourier series theory** and uses the reference signal to extract from the signals the amplitude and phase of each multiple component of the reference. This method is very effective each time is present inside a signal one or more coherent components related to a reference with a phase relation and a multiple periodicity.

The signals sampled during the experiment have a part f(t) due to the injection from the active magnetic bearings:

$$f(t) = a_0 + \sum_{n=1}^{\infty} a_n \cos(n\omega_0 t) + b_n \sin(n\omega_0 t) \tag{13}$$

Where $\omega_o = \frac{2\pi}{T}$ and l=T/2

Performing the integration along one or more periods, the Fourier theory computes the amplitude components as:

$$a_0 = \bar{f} = \frac{1}{T}\int_{t_0}^{t_0+T} f(t)dt \tag{14a}$$

$$a_n = \frac{1}{l}\int_{t_0}^{t_0+T} f(t)\cos(n\omega_0 t)dt \tag{14b}$$

$$b_n = \frac{1}{l}\int_{t_0}^{t_0+T} f(t)\sin(n\omega_0 t)dt \tag{14c}$$

Using the trigonometric relations the equations became:

$$A_n = \sqrt{\left(a_n^2 + b_n^2\right)} \qquad \phi_n = \tan^{-1}\frac{b_n}{a_n} \tag{15}$$

$$f(t) = a_0 + \sum_{n=1}^{\infty} A_n \cos(n\omega t - \phi_n) \tag{16}$$

With this notation, positive ϕ_n represent a phase lag. In the solution of the dynamic equations the phase representation has to be consistent with the phase from the experimental data.

The rejection of the filter with respect to other non-synchronous components or noise depends on the number of periods used for the integration. For the experiment, the number of periods were the integer periods included inside the 0.8s analysis window and they are about 22 for the 28Hz tone (1X), about 56 for the 70Hz tone (2X), 101 for the 126Hz tone (9X), 146 for the 182Hz (11X) and 190 for the 238Hz tone (17X) (see Figure 11 and Figure 12).

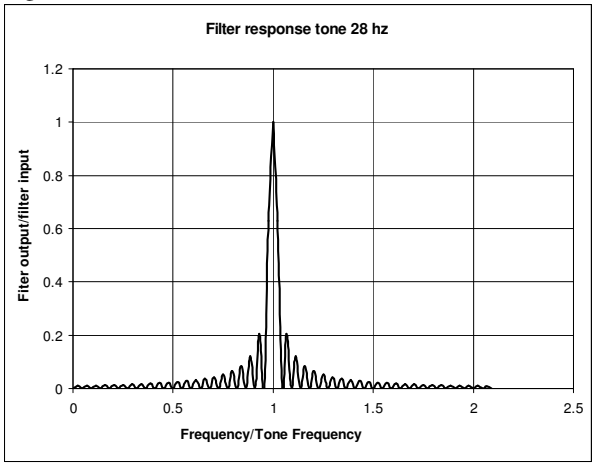

Figure 11 – Aspect of filter function on first tone.

Copyright © 2011 by Turbomachinery Laboratory, Texas A&M University

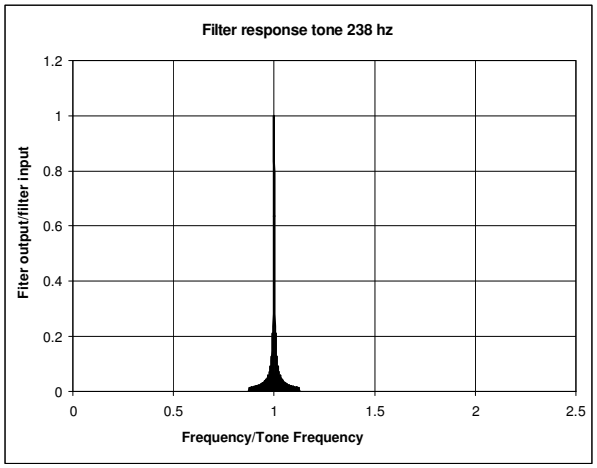

Figure 12 – Aspect of filter function of fifth tone.

The use of this algorithm to extract amplitude and phase for each component of the signal of interest allows computing in real time the parameters and performing trending during the experiment. Using the amplitude and phase for each component, then the visualization of **orbits filtered on each frequency** is performed. This allows during the experiment to set the proper rotor orbits (Figure 13) and check if the contribution of each component remains steady.

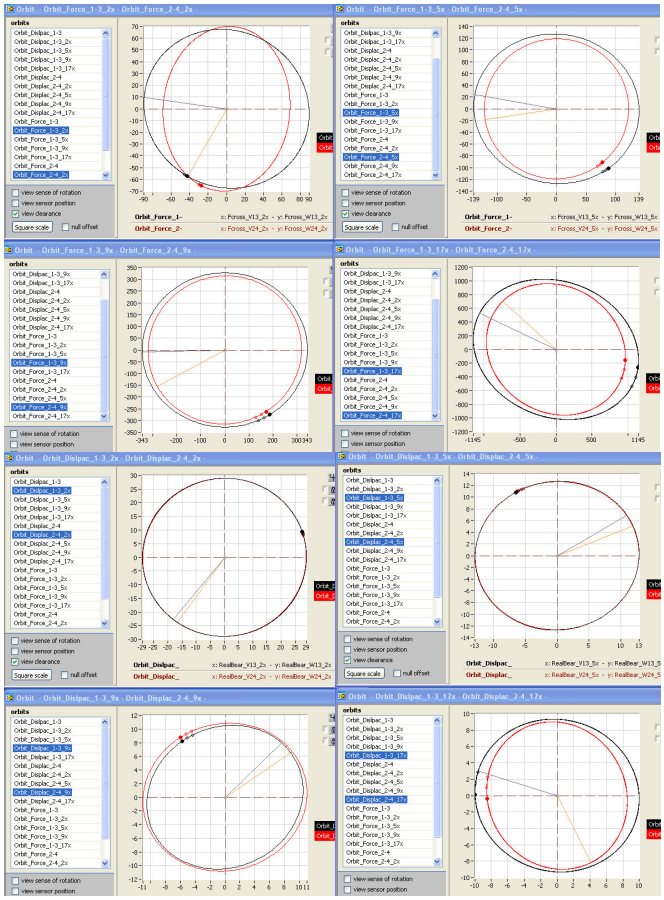

Figure 13 – Orbit plots of forces and displacements.

Seal Coefficients identification

After extraction of displacements and forces for each tone, the amplitudes and phases are imported inside a code developed that performs the following operations:

- Import of the displacement and force vectors
- Correction of the force and displacements vectors using the dynamic calibration data
- Correction of the displacement vectors for the stator vibration contribution (for the inertia computation)
- Baseline coefficients identification (without gas condition)
- Experiment coefficients identification
- Subtraction of the baseline to the experiment

Finally, the code computes the coefficients as trend lines during all the experiment to facilitate the diagnosis of a possible noisy experiment and to eventually discard not reliable test points. The error computation is then performed as described later on.

Sensors

The main signals to be measured for the seal coefficients identification are the rotor displacements and the currents that drive the Active magnetic Bearings coils.

As described above, these signals are then used to compute the position of the rotor in the sealing section (sensors and sealing are not co-located) and the accelerations of the center of gravity. The currents are used (together with the position) for the force formulation.

Current sensors are additional with respect to the standard ones of the Magnetic Bearing controller; The sensors were chosen to achieve the accuracy of 0.05A.

The displacement sensors are the original sensors from the magnetic bearing panel; these sensors are of differential inductive type and have a resolution of 0.1 µm. This level of accuracy was achieved through an extensive calibration effort, as it will be described in the next section.

Calibrations

A dedicated calibration has been performed for each vital measurement in order to refer the measurements to international standards. The uncertainty associated with each measurement was identified and used finally as input for an error propagation analysis, the dynamic correction as the vibration of the stators and the uncertainty computation. Starting from the point that all the commercial transducers were calibrated, on the main parameters collected for the seal coefficient determination (the 4 rotor displacements and the 4 Forces actuated by the Active Magnetic Bearing which are computed by measuring the currents and the position of the rotor inside the bearing gap) a dedicated calibration was performed on the test rig.

Static Calibration - Forces

The static force calibration was needed to tune the parameters of the force transfer function; for this reason the calibration procedure is based on different loads at different position of the shaft. Finally, the parameters that are adjusted are the gap g and the surface A_t (see equation 9). To perform a calibration not affected by hysteresis phenomena, the calibration procedure is performed first increasing the load and then decreasing the load and comparing the results.

Moreover, the verification of the applied force axis direction was done. This was made possible by a dedicated

Copyright © 2011 by Turbomachinery Laboratory, Texas A&M University

fixture where the loads (weights) were applied to the rotor through steel wires positioned at +45° and – 45° with respect to the vertical direction (red and blue lines of Figure 14)

Specifically, the calibration rig consists of a frame structure able to sustain a set of 8 pulleys which realize crosses of steel wires which are connected to both shaft ends. Calibrated weights are then connected to apply the static loads.

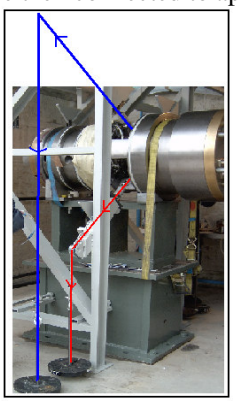

Figure 14 – Calibration of AMBs static forces and relevant direction.

The use of wires allows to apply the static forces in any position of the shaft and allows checking the direction of the forces. Previous calibration rigs used oil pistons and load cells, but the results were not good due to the uncertainty of the force direction and the difficulty to realize calibrations with the rotor out from the centerline.

The effect of the position and the saturation are assessed within an uncertainty of 25 N with 95% confidence level.

The air gap which was tuned to match the static forces applied was greater than the geometrical gap of the bearing. (1mm is the geometrical gap while 1.2mm is the adjusted gap).

Static Calibration – Displacements

As per force calibration, also the displacement sensors were calibrated to take care of amplitude corrections but also to get the correct directions.

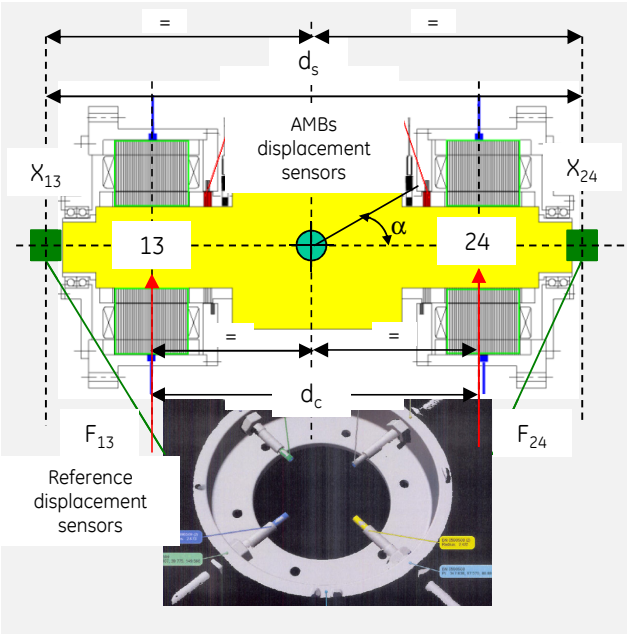

Figure 15 – Displacement sensors calibration fixture.

To check also the directions we used a set of 4 reference proximity probes (eddy current probes) for each end of the shaft, placed each 90°.

The results (Figure 16) were very important to detect an uncertainty of the bearing displacement measurement system that showed a configuration of the sensors not exactly at 90° to each other.

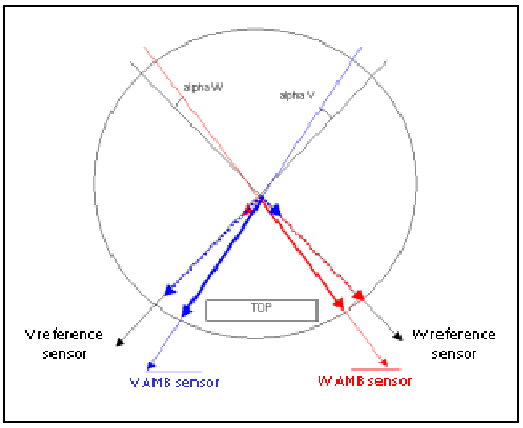

Figure 16 – Displacement Sensors direction check.

The correction formulas used are described in the following:

$$X_{v_\perp} = X_v \cos\alpha_v + X_w \sin\alpha_w$$
$$X_{w_\perp} = X_w \cos\alpha_w + X_v \sin\alpha_v \qquad (17)$$

With the following angles:

alpha	
V13 (deg) 5.9	**V24 (deg)** 4.0
W13 (deg) 4.2	**W24 (deg)** 3.7

Table 2 – Correction angles for displacement sensors calibration.

The check for the exact direction of both the forces and displacements is very important because an inaccurate axis direction can cause a mixing of the effects of the direct coefficients (inertia included) with the cross coupled coefficients.

The reason why the displacement sensors are not exactly 90° spaced is under investigation.

Dynamic calibration – Forces and displacements

Finally, a dynamic calibration was performed to take into account the following contributions:

1) Bandwidth of the measurement chains
2) Bandwidth of the exciter (forces are computed from the currents) and the transfer function needs a calibration in frequency
3) Stator vibrations
4) Displacement sensors support vibrations

To perform this calibration, accelerometers were installed both on the rotor (at both shaft ends) and on the stator, along the V and W axes. Injecting on each axis sinusoidal signals at different frequencies, accelerations were acquired; taking care

Copyright © 2011 by Turbomachinery Laboratory, Texas A&M University

of the proper collocation of the sensors, the rotor displacement computation (through the accelerations) was done with a double integration, and angular acceleration was computed as the second derivative of α, where:

$$\alpha = \arctan\left(\frac{x_{13} - x_{24}}{d_s}\right) \tag{18}$$

The calibration displacements at the AMB sensor location were computed simply subtracting the displacement of the stators to the displacement of the rotor.

The calibration forces at the AMB location 13 and 24 were obtained from the rotor equation of motion:

$$f_{13} = M_R \cdot \frac{(\ddot{x}_{13} + \ddot{x}_{24})}{4} - \frac{I_R \cdot \ddot{\alpha}}{d_c}$$

$$f_{24} = M_R \cdot \frac{(\ddot{x}_{13} + \ddot{x}_{24})}{4} + \frac{I_R \cdot \ddot{\alpha}}{d_c} \tag{19a, b}$$

For the symbols explanation see Nomenclature and Figure 15. Eqs. 19a, b are based on following assumptions:

- Rigid rotor
- Negligible gyroscopic effects

The displacement measured with the AMB sensors were calibrated with the reference displacements at any frequency. The forces computed with the AMB currents were calibrated with the reference forces at any frequency; the results showed saturation for the forces and a mismatch between the measured displacements versus the real displacements due to displacements sensor support vibrations. The casing vibrations were checked to be negligible.

The calibrations were finally used in the data postprocessing.

Considering all the calibrations introduced into the measurements, the system is finally able to have an uncertainty on the displacements of +/-1μm (+/- 3% of the reading) and +/-25N (+/-6% of the reading), with a 95% confidence level.

Signal generation setting

To measure forces and displacement at many different frequencies the selected experiment method was to generate an excitation signal with a specific frequency content which is called pseudorandom or multitone excitation.

This method consists in the generation of a waveform, which is the sum of several pure sinusoids with different frequencies. Then the phasing between the pure sinusoids injected on each axis is able to create either the vertical or the horizontal or the circular whirl. In more details with a phase shift of 0° we impose a vertical orbit, with a 180° we impose a horizontal, with a 90° lag we impose a circular forward and with a 90° lead we impose a circular backward.

For the all the tests performed a reference signal of 14Hz was selected and 5 tones at 2X, 5X, 9X, 13X and 17X were generated. This harmonic selection was done in order to avoid that one frequency was multiple of another and to avoid that a frequency was matching the rotational speed (three rotational speed were used: 6000rpm-10000rpm-15000rpm).

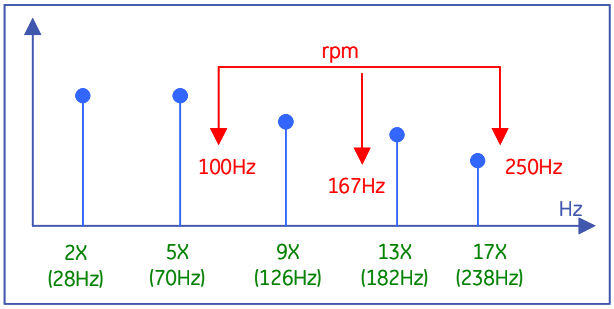

Figure 17 – Multitone excitation signal generation.

In this way also in case of non-linear behaviours, the second and other harmonics of the excitation tones are not interfering each other.

The setup of the injected waveform is performed just before the experiment; with a control console the tones are added for each axis of each Magnetic Bearing

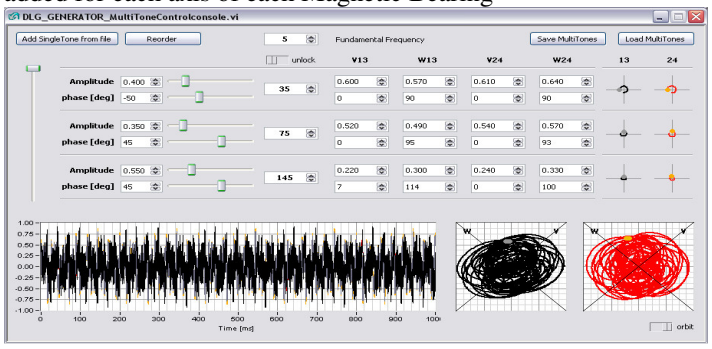

Figure 18 – Control console to create the excitation signal.

The waveform visualization for each axis is not representative and helpful to understand the whirl on each tone, so in order to set the required whirling motion the data recorder by the Dynamic Data Acquisition system were used: the real time spectral analysis and the real time digital vector filtering that allow to have filtered orbits on the monitoring system were in fact used.

Final uncertainty computation

The measurement uncertainties are finally propagated in the computation with the following approach: each input parameter is perturbed with the known uncertainty and the effect on the output is stored. Then all the effects are added with a mean squared approach. The logic diagram is shown below.

Copyright © 2011 by Turbomachinery Laboratory, Texas A&M University

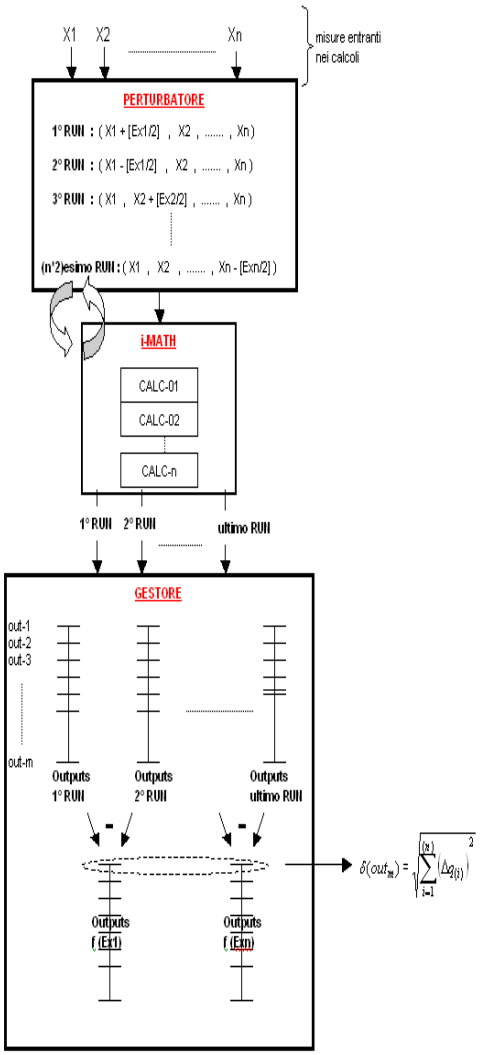

Figure 19 – Uncertainty propagation logic diagram.

TEST RESULTS

The test campaign is still in progress at the time; specifically the tests with inlet pressure higher than 200bar are still pending. In the present paragraph the test results relevant to 10krpm rotational speed and the following pressure levels will be shown (pressure levels refer to test cell inlet and exit):

- Test#1: 50 – 25bar
- Test#2: 100 – 50bar
- Test#3: 200 – 100bar

The preswirl value is estimated to be 0.85 at 10krpm so this dataset is representative of a high preswirl condition (balance piston seal working without shunts or swirl brakes).

Temperatures upstream the seal are measured in the range 15-20°C for all the three test points.

At first the different excitation methods are compared: Horizontal and Vertical linear excitations and Forward + Backward circular orbit (based on Test#3 conditions). Figure 20 shows that all the three methods are in good agreement within a 30% difference (considering the subsynchronous tones only) for what is concerning the cross coupled stiffness. Figure 21, which is relevant to the direct damping, shows more difference among the three methods: up to 80% between the horizontal method experiments and the Vertical (or Forward + Backward which is consistent with the Vertical).

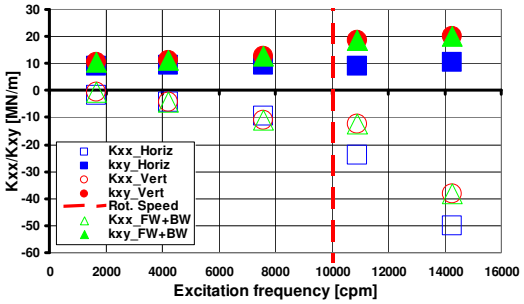

Figure 20 – Comparison of stiffness coefficients from different excitation methods.

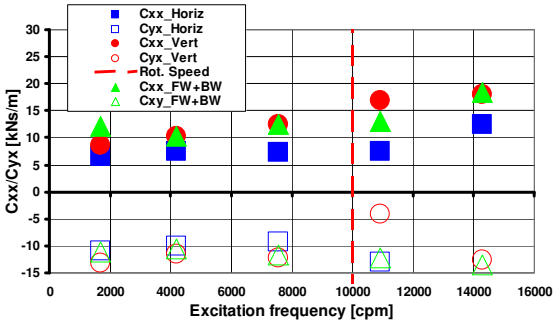

Figure 21 - Comparison of damping coefficients from different excitation methods.

In the following all the results showed are relevant to one kind of excitation only (horizontal) since the comparison mentioned above proved that they are overall equivalent. Results from all the three test cases are shown.

Figure 22 and Figure 23 show the stiffness and damping coefficients (both direct and cross coupled) for the three different pressure levels (Test #1, #2, #3). All the coefficients are consistently increasing with the pressure level. The strongest trend with pressure is associated with the direct stiffness, especially at the two higher tones (which are anyway associated to the highest experimental uncertainty).

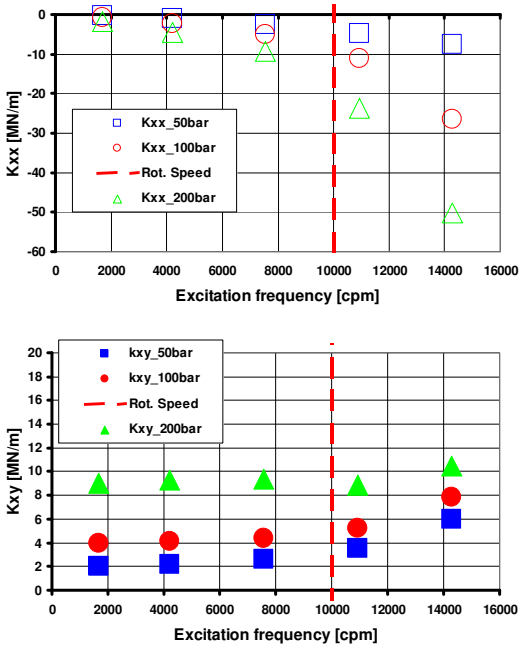

Figure 22a,b–Stiffness coefficients comparison for different pressure levels.

Copyright © 2011 by Turbomachinery Laboratory, Texas A&M University

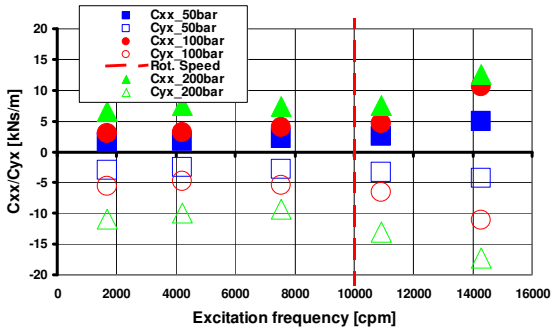

Figure 23 – Damping coefficients comparison for different pressure levels.

Finally a comparison with predictions is shown in the rest of the paragraph. As far as it is concerning the predictions the XLLaby tool developed by Childs and Thorat, 2009 was used. This tool allows for advanced selection options like:

- Frequency dependence coefficients calculation
- Leakage equation selection
- Variable clearance along the seal length (depending on the leakage equation selected)

For all the predictions showed below the Neumann leakage equation was selected together with a frequency dependent – constant clearance modelization. Figure 24 a, b and Figure 25 a, b show the comparison between measurements and predictions for Test#3 case. It is important to notice that that the predicted cross coupled coefficients are bounded with a +/-20% preswirl uncertainty line, which corresponds to the current capability of the test rig to detect the preswirl parameter. Since the predictions (especially the cross-coupled stiffness) are very sensitive to this parameter, the relevant uncertainty was taken into consideration for sake of precision in the comparison.

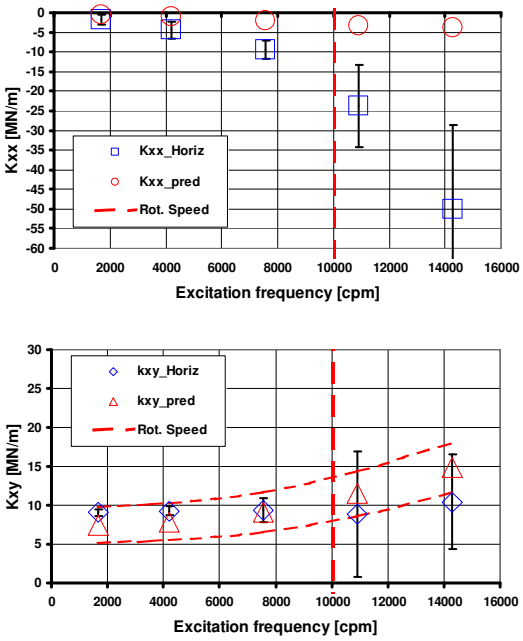

Figure 24a, b – Stiffness coefficients: measured vs. predicted.

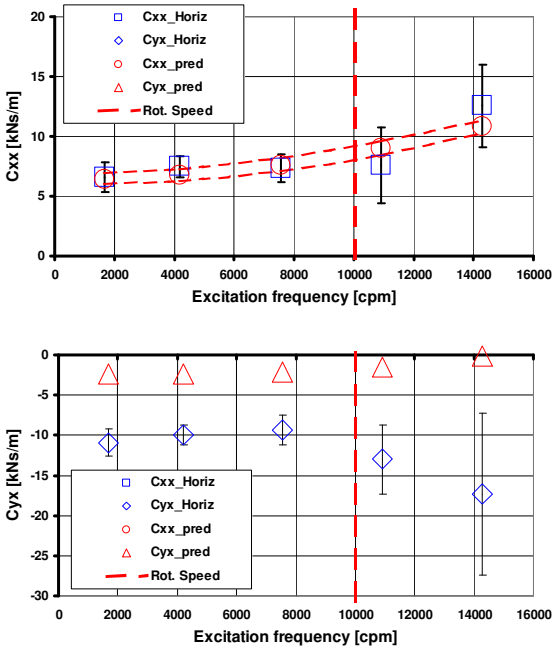

Figure 25 a,b – Damping coefficients: measured vs. predicted.

The agreement between the measured and predicted coefficients is generally very good; the main considerations are summarized as follows:

- Direct stiffness (Figure 24 a): the experimental trend seems to be much more sensitive to the excitation frequency anyway this happens with the high frequency tones, which are characterized by the highest experimental uncertainty.
- Cross-coupled stiffness (Figure 24 b): the agreement between predictions and test data is within 15% difference.
- Direct damping (Figure 25 a): the agreement between predictions and test data is within 10% difference.
- Cross-coupled damping (Figure 25 b): the test data are generally higher than the predictions showing comparable values with the direct damping.

CONCLUSIONS

The present paper describes in full details the capabilities of the authors' Company seal test rig facility, which was built to increase the level of understanding in the seal dynamics behaviour and the confidence in the relevant predictive tool.

Currently the test rig is fully operational and the first test campaign is in progress. The test object is a long labyrinth seal. The current test results (inlet pressure levels within 200bar) are confirming that the labyrinth seal coefficients which are more strictly related to the rotordynamic stability (namely k and C) are lightly dependent on the excitation frequency and, more important, they are well predicted by the current numerical tools (the agreement is within 15%).

More test results are now coming (pressure levels up to 350bar) and after this test campaign it will be possible to move to different seal types (damper seals) using the current test data either to assess the reliability of the long labyrinth seals predictive tool or to define a baseline for the future seals.

Copyright © 2011 by Turbomachinery Laboratory, Texas A&M University

NOMENCLATURE

AMBs: Active Magnetic Bearings
AMB#13: drive end magnetic bearing
AMB#24: not drive end magnetic bearing
A_t: the magnetic core area
$[A]_{(exp)}$: matrix of coefficients measured during experiment
B: magnetic flux density [N/(A·m)]
$[B]_{(exp)}$: know terms array measured during experiment
$[B]_{(baseline)}$: know terms array measured during baseline
C: seal direct damping [Ns/m]
C: seal cross coupled damping [Ns/m]
d_s: distance between accelerometers [m]
d_c: distance between AMB midplanes [m]
F_{bx}, F_{by}: forces due to AMBs [N]
F_{kx}, F_{ky}: forces due to seal stiffness terms [N]
F_{cx}, F_{Cy}: forces due to seal damping terms [N]
$F_{bx0,}$ F_{by0}: amplitude of force due to AMB [N]
g, $g_{effective}$: nominal and effective gap between the Active Magnetic Bearing expansion and the rotor
H: magnetic field strength [A/m]
HMI: Human Machine Interface
I_{TOP}, I_{BOTTOM}: currents inside the windings
I_R: rotor transverse moment of inertia at rotor center of gravity [kg*m^2]
K: seal direct stiffness [N/m]
K: seal cross coupled stiffness [N/m]
L1, L2, L3, L4: magnetic circuit lengths [m]
LOTO: Lock Out Tag Out
M_R: rotor mass [kg]
N: number of windings
PCV: Pressure Control Valve
PED: Pressure Equipment Directive
UCP: Unit Control Panel
x_{13}, x_{24}: rotor displacement in the x direction measured by accelerometers placed at both shaft ends [m]
x: rotor displacements measured at AMB sensors in the x direction [m]
x_0, y_0: amplitude of displacement [m]
y_{13}, y_{24}: rotor displacement in the y direction measured by accelerometers placed at both shaft ends [m]
y: rotor displacements measured at AMB sensors in the y direction [m]
$\alpha, \dot{\alpha}, \ddot{\alpha}$: rotor angular degree of freedom [-,1/sec,1/sec^2]
Ω: precession frequency (rad/sec)
ω: rotational frequency (rad/sec)
ω: rotational frequency (rad/sec)
Φ_x, Φ_y: phase of displacement [rad]
Φ_{bx}, Φ_{by}: phase of force due to AMB [rad]
μ_r: material relative magnetic permeability [N/A^2]
μ_0: vacuum magnetic permeability [N/A^2]

REFERENCES

API 617 7th Edition, July 2002, "Axial and Centrifugal Compressors and Expander-compressors for Petroleum, Chemical and Gas Service Industry".

Baumann, U., 1999, "Rotordynamic Stability Test on High Pressure Radial Compressors", Proceedings of the 28th Turbomachinery Symposium", Turbomachinery laboratory, Texas A&M University, College Station, Texas, pp.115-122.

Childs, D., Scharrer, J., "An Iwatsubo based solution for labyrinth seals: comparison to experimental results", Journal of Engineering for Gas Turbines and Power, April 1986, Vol. 108, pp. 325-331.

Cochrane, 1976, "New generation compressor injecting gas at Ekofisk, Oil&Gas Journal, pp. 63-70.

Fulton J.W., "The decision to full load test a high pressure centrifugal compressor in its module prior to tow-out", I Mech E., 2nd European congress on "Fluid machinery for the oil, petrochemical and related industries", The Hague, The Netherlands, March 1984.

Iwatsubo, T, Takahara, K., Kawai, R., "A new model of labyrinth seal for prediction of the dynamic force", Proceedings of a workshop at Texas A&M University 28-30 May 1984, Entitled Rotordynamic Instability Problems in High Performance Turbomachinery, pp. 1-16.

Kocur, J., Nicholas, J., Lee, C., 2007, "Surveying tilting pad journal bearing and gas labyrinth seal coefficients and their effect on rotor stability", Proceedings of the 36th Turbomachinery Symposium, Turbomachinery Laboratory, Texas A&M University, College Station, Texas, pp. 1-10.

Moore, J., Walker, Kuzdzal, "Rotordynamic Stability Measurement during full load", Turbomachinery Symposium 2002, pp. 29-38.

Picardo, A. and Childs, D., "Rotordynamic coefficients for a Teeth-on-Stator Labyrinth Seals at 70 bar Supply Pressures-Measurements Versus Theory and Comparisons to a Honeycomb Seal," ASME J. of Gas Turbines, October 2005, 127 , pp. 843-855.

Rouvas, C. and Childs, D., 1993, "A Parameter Identification Method for the Rotordynamic Coefficients of a High Reynolds Number Hydrostatic Bearing," ASME J. of Vibration and Acoustics, 115, pp. 264-270.

Smith, K. J., 1975, "An operation history of fractional frequency whirl", Proceedings of the 4th Turbomachinery Symposium, Turbomachinery Laboratory, Texas A&M University, College Station, Texas, pp. 115-125.

Thorat, M., Childs, D., 2009, "Predicted rotordynamic behavior of a labyrinth seal as rotor surface velocity approaches Mach 1", Paper GT2009-59256, Proceedings of ASME International Gas Turbine Institute Turbo Expo, Orlando, USA 2009.

Wagner, N. G., Steff, K., 1996, Dynamic labyrinth coefficients from a high pressure full scale test rig using magnetic bearings, Rotordynamic Instability problems in high performance turbomachinery, NASA Conf. Publ. 3344, pp. 95-112.

Wagner, N. G., Steff, K., Gausmann R., Schmidt M., Investigations on the dynamic coefficients of impeller eye labyrinth seals, Proceedings of the 38th Turbomachinery Symposium, Turbomachinery Laboratory, Texas A&M University, College Station, Texas, pp. 53-70.

ACKNOWLEDGEMENTS

The authors gratefully thank the Company for the permission to publish the test data and to give their contribution to the knowledge sharing in the rotordynamic technical community.

Copyright © 2011 by Turbomachinery Laboratory, Texas A&M University